Extra metal adatom surface diffusion simulation on 1/3 ML Si(111) $\sqrt{3} \times \sqrt{3}$ metal-induced surfaces

2013 Phys. Scr. 88 035604

(http://iopscience.iop.org/1402-4896/88/3/035604)

Phys. Scr. **88** (2013) 035604 (8pp) doi:10.1088/0031-8949/88/03/035604

Extra metal adatom surface diffusion simulation on 1/3 ML Si(111) $\sqrt{3} \times \sqrt{3}$ metal-induced surfaces

Yu V Luniakov

Institute of Automation and Control Processes, Far Eastern Branch of Russian Academy of Sciences, 690041 Vladivostok, Russia
School of Natural Sciences, Far Eastern Federal University, 690950 Vladivostok, Russia

E-mail: luniakov@iacp.dvo.ru

Received 3 April 2013
Accepted for publication 30 July 2013
Published 22 August 2013
Online at stacks.iop.org/PhysScr/88/035604

Abstract
A first-principle simulation of the surface diffusion of an extra metal (Me) adatom has been performed on the corresponding 1/3 monolayer (ML) Si(111) $\sqrt{3} \times \sqrt{3}$ Me-induced surfaces. Using the nudged elastic band (NEB) optimization method, the minimum energy paths and the activation energy barrier profiles for all known Me-inducing $\sqrt{3} \times \sqrt{3}$ reconstruction on an Si(111) surface at the 1/3 ML coverage have been obtained and compared with the available experimental data. The activation barrier is shown to depend on the atomic size of the diffusing adatom: the barrier has the highest value for the largest Me adatom, Pb (0.44 eV); lower values for the smaller Me adatoms, Sn (0.36 eV), In (0.22 eV) and Ga (0.13 eV); and the lowest value for the smallest Me adatom, Al (0.08 eV). The Arrhenius pre-exponential factors that were obtained in the harmonic approximation are as large as $\sim 10^{11-13}$ Hz for all of the investigated surfaces, which supports the single-adatom diffusion model considered here.

PACS numbers: 68.35.bg, 68.55.Ln

(Some figures may appear in colour only in the online journal)

1. Introduction

Diffusion is a transport phenomenon that attracts much interest from experimenters and theorists because it is responsible for different fundamental processes at the surface of a solid and in its bulk. As shown by Brihuega *et al* [1], single-adatom diffusion can be experimentally examined with atomic resolution on an atomically clean defect-free Pb-induced Si(111) $\sqrt{3} \times \sqrt{3}$ surface. In their consequent work, Brihuega *et al* [2] have identified the nature and the adsorption sites of the additional Pb adatoms and accurately determined the diffusion parameters of one extra Pb adatom on this surface. The measurement of the hopping rates over a temperature range from 145 to 165 K provided the activation energy value $E_d = 0.45 \pm 0.01$ eV and the Arrhenius prefactor $\nu_0 = 10^{13.0 \pm 0.4}$ Hz. The question is whether the diffusion mechanism is as simple as that deduced from the scanning tunneling microscopy (STM) images. Can other atoms contribute to the atomic diffusion that was observed in the STM? The experimental data cannot provide a clear answer to this question: in general, only notably accurate, time-consuming simulations can clarify the mechanism that is actually responsible for the observed diffusion phenomenon. This paper investigates the mechanism of a single extra metal (Me) adatom diffusion on all known Me-induced Si(111) $\sqrt{3} \times \sqrt{3}$ surfaces with identical structure, which are formed at 1/3 ML of a monolayer (ML) of Me coverage, using modern density functional theory (DFT) simulation tools.

The Si(111) $\sqrt{3} \times \sqrt{3}$ 1/3 ML Me-induced surface that was chosen for the investigation is a notably popular model system, and it might be expected to be one of the best-understood reconstructions in surface science. In the $\sqrt{3} \times \sqrt{3}$ 1/3 ML structure, there is one Me adatom among three neighbouring T_4 sites of the bulk-terminated Si(111)-1×1 layer, which occupies the threefold symmetric T_4 site above the second-layer Si atoms, as shown in figure 1. This type of structure is formed on the Si(111) surface by group-III Me atoms (Al, In, Ga), group-IV Me atoms (Pb and

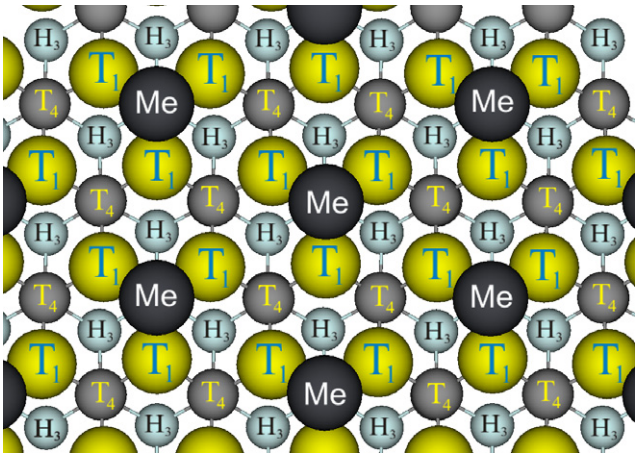

Figure 1. Structural model of the Me-induced Si(111) $\sqrt{3} \times \sqrt{3}$ surface with Me adatoms occupying the T_4 cites. The Me atoms are depicted with large black circles, the topmost Si atoms of the first layer are depicted with large yellow circles, the second-layer Si atoms are depicted with grey circles and the fourth-layer Si atoms are depicted with small cyan circles. The adsorption sites T_1, T_4 and H_3 are marked with text labels.

Sn) and a group-V Me atom (Bi) [3]. The structure of this type of surface reconstruction has been known since the end of the last century because of a number of pioneering theoretical papers of Chelikowsky [4] and Northrup [5] for Al; Meade and Vanderbilt [6], and Zegenhagen *et al* [7] for Ga; Nicholls *et al* [8] for In; Chan *et al* [9] for Pb; Ramchurn *et al* [10] for Sn; and Cheng and Kunc [11] for Bi. The theoretical papers supported a large amount of experimental observations that were accumulated by that time [3].

The theoretical diffusion parameters, such as the activation energy and especially the Arrhenius prefactor, which is determined from the phonon frequencies, are notably dependent on the calculation details such as the precision and the exchange correlation potential. The local density approximation (LDA) usually results in a realistic description of the structural, elastic and vibrational properties, but the binding and cohesive energies are often overestimated. The generalized gradient approximation (GGA) gives a more realistic description of the energy barriers in the dissociative adsorption of hydrogen on Me and semiconductor surfaces [12, 13]. In some cases, LDA calculations yield better consistency with the experiments than GGA calculations [14, 15]. For example, in the case of Si surfaces, this is simply an artefact of a delicate balance between the exchange and the correlation, which results in a large error compensation. It is sometimes difficult in advance to choose between the LDA and the GGA exchange-correlations, particularly if there are different available GGA types. Different modifications of GGA have usually been used to simulate the adsorption of Me on silicon surfaces, but LDA is also known to provide notably correct results in many cases. For example, Chan *et al* [9] used LDA to study the stability of different structures that were formed with Pb adatoms on an Si(111) surface, whereas Jia *et al* [16] used the GGA PW91 to simulate the Pb Me films. Northrup [5, 17] applied a simple LDA approach in his pioneering papers to calculate the Si(111) $\sqrt{3} \times \sqrt{3}$–Al surface structures, whereas Teng *et al* [18] preferred to use the GGA for a ML Al film investigation. Dai *et al* [19] used LDA to study the atomic structures of an In atom on an Si(100)-2×1 surface, Ervin *et al* [20] used LDA to simulate a Ga vacancy interaction on an Si(112) surface and Yeom *et al* [21] used GGA to calculate the electronic structure of Ga overlayers on Si(111) surfaces. Profeta *et al* [22] used LDA to study Sn alloying on an Si(111) surface and revealed the importance of the many-body electron correlation effects for Sn/Si(111) and Sn/Ge(111) systems. Koroteev *et al* [23] used LDA to investigate ultrathin Bi films, and Cheng and Kunc [11] used LDA to investigate the structure and the stabilities of Bi layers on Si(111) and Ge(111) surfaces, whereas Owen *et al* [24] used the GGA PW91 to simulate a Bi nanoline on an Si(100)-$p(2 \times 2)$ surface. It is often highly recommended to perform a test of the dependence of the calculation results on the chosen exchange-correlation potential because the calculation results also depend on the quality and the transferability of the pseudopotentials [25]. To examine the influence of the exchange correlation functional used for the calculations, the dependence of the obtained results on the choice of the form of the exchange-correlation potential is briefly investigated at the end of section 3.2.

2. Methods of calculations

The plane-wave total energies in this work were calculated using the Vienna *Ab Initio* Simulation Package (VASP) [26–29] based on the DFT [30, 31]. The electronic ground state of the system was calculated using the projector-augmented wave [32, 33] potentials as provided in VASP. The LDA after Ceperley–Alder [34] in the Perdew–Zunger parameterization [35] for the exchange and correlation functional was employed.

The supercell geometry of a repeating slab separated by a vacuum region, which was not less than 10 Å, was used in this study. Each slab comprises six atomic layers of Si and one Me adsorbate layer on the top surface. All atoms were allowed to relax except the bottom two silicon layers, which were constrained to remain in bulk-like positions. H atoms were attached to the bottom-layer Si atoms to saturate their dangling bonds. The activation energies for an extra Me adatom diffusion were calculated using the nudged elastic band (NEB) method [36, 37], which calculates the diffusion barrier between two known minimum energy sites by optimizing the number of intermediate images or snapshots of the adatom along the diffusing path. To ensure the continuity of the path, a spring interaction between adjacent images is added, which forms an elastic band. To calculate the barrier, the atomic positions in each image are fully relaxed until a force convergence to 10^{-2} eV Å^{-1} is achieved, and the image that corresponds to the highest energy is taken to be the top of the diffusion path. Because the reaction path shape is not linear, a climbing-image NEB method was used to search for the saddle points [38], where the highest-energy image is driven up to the saddle point. Because the accuracy of the determination of the first-order transition state (FOTS) is important for the prefactor calculation, the dimer method [39, 40] was applied to find them.

The wave functions were expanded using a plane-wave basis with an energy cutoff $E_{\mathrm{cut}} \geqslant 250$ eV, and the 'accurate' value of the precision-control tag provided by VASP was used.

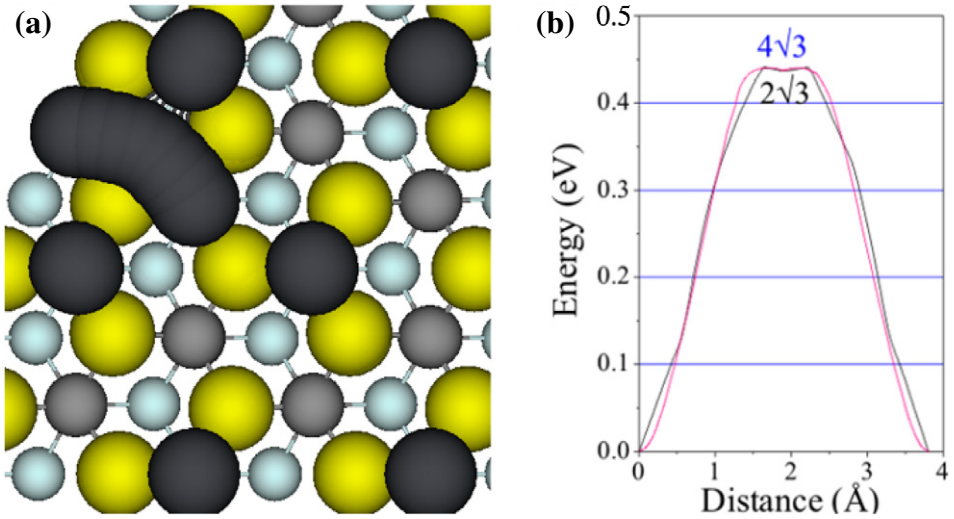

Figure 2. (a) The minimum energy path of the extra Pb adatom diffusion on the Pb-induced Si(111) $\sqrt{3} \times \sqrt{3}$ surface, which was obtained using NEB optimization, and (b) the corresponding energy profiles for the $2\sqrt{3} \times 2\sqrt{3}$ and $4\sqrt{3} \times 4\sqrt{3}$ supercells. The designations are identical to those in figure 1.

The Brillouin zone integration was performed with a Γ-point for the large supercells $4\sqrt{3} \times 4\sqrt{3}$ and $6\sqrt{3} \times 6\sqrt{3}$ and with a series of k-points that originated from the Δ-one (0.25, 0.25, 0) for the smaller supercell $2\sqrt{3} \times 2\sqrt{3}$. The geometry was optimized until the total energy converged to 10^{-4} eV and the total force converged to 10^{-2} eV Å^{-1}. The dependence of the activation energy on the kinetic energy cutoff, the k-points number and the number of Si layers was examined and found to have a negligible effect on the total energy differences. The dependence of the activation energy on the number of $\sqrt{3}$ cells in the supercell was also investigated, which showed that a $4\sqrt{3} \times 4\sqrt{3}$ supercell size was sufficiently large for all calculations (see section 3.1).

3. Results and discussion

3.1. Choice of the supercell size

Because all of the Me-induced Si(111) $\sqrt{3} \times \sqrt{3}$ surfaces for Me = Al, Ga, In, Sn, Pb and Bi have identical atomic arrangement, an identical atomic model, which is shown in figure 1, can be used to simulate their extra Me adatom diffusions. To check the dependence of the activation energy on the size of the supercell, a series of NEB calculations of the diffusion of an extra Pb adatom on an Si(111) $N\sqrt{3} \times N\sqrt{3}$–Pb supercell was performed, where $N = 2$, 4 and 6. The extra Pb adatom was moving from one equilibrium T_4 position to the neighbouring T_4 site through a number of snapshots that lay on the straight line that connected these two positions. The initial straight-line path after the NEB optimization was transformed to a curve that passed around the first-layer Si atom T_1 through the hollow H_3 site, as shown in figure 2(a). All calculations were performed using different sets of k-points that originated from the Δ-one at (0.25, 0.25, 0) and the Γ-point at (0, 0, 0). Table 1 summarizes the resulting activation energies, which were calculated as the difference between the total energies of the system with the extra Pb adatom in the saddle point and those of the system with the extra Pb adatom in the equilibrium T_4 position.

Table 1. The dependence on the supercell size of the activation energies (in eV) for an extra Pb adatom diffusion on the Pb-induced Si(111) $\sqrt{3} \times \sqrt{3}$ surface.

Supercell size	$2\sqrt{3} \times 2\sqrt{3}$			$4\sqrt{3} \times 4\sqrt{3}$		$6\sqrt{3} \times 6\sqrt{3}$
k-points set	2×2	1×1	1	1×1	1	1
k-points origin	Δ	Δ	Γ	Δ	Γ	Γ
Energy barrier (eV)	0.44	0.43	0.39	0.44	0.44	0.45

We observe that even when the supercell is as small as $2\sqrt{3} \times 2\sqrt{3}$, the activation energy is almost identical to that for larger supercells such as $4\sqrt{3} \times 4\sqrt{3}$ and $6\sqrt{3} \times 6\sqrt{3}$. Because the Γ-point calculations give notably reasonable results for large supercells, the Γ-point calculations were performed for the $4\sqrt{3} \times 4\sqrt{3}$ supercell to simulate the extra Me adatom diffusion.

3.2. Saddle points and transition states calculation

Independently of the form of the initial trial path, the resulting NEB-optimized path of the extra Me adatom diffusion goes around the first-layer Si atom T_1 through the hollow H_3 site similarly to the path shown in figure 2(a). For ease of visualization, the distances traversed by the extra Me adatom were projected to the line that connected the neighbouring T_4 sites, so that the entire distance was equal to the Si surface lattice period 3.82 Å, which was provided by the corresponding LDA exchange-correlation potential. The path obtained after only six to eight images from the linear trial path reproduces the main diffusion profile features such as the location and the energy of the transition states. The diffusion path retains a reflection symmetry about the plane that passes through the occupied T_4 sites perpendicular to the path (the red line in figure 3(a)) because all of the investigated Si(111) $\sqrt{3} \times \sqrt{3}$–Me surfaces have the same symmetry. The saddle points are also symmetrical about this plane, and they are separated from one another by 0.6–0.8 Å for the larger Me adatoms such as Pb, Sn and In and by 2.2–2.6 Å for the smaller Me adatoms such as Ga and Al.

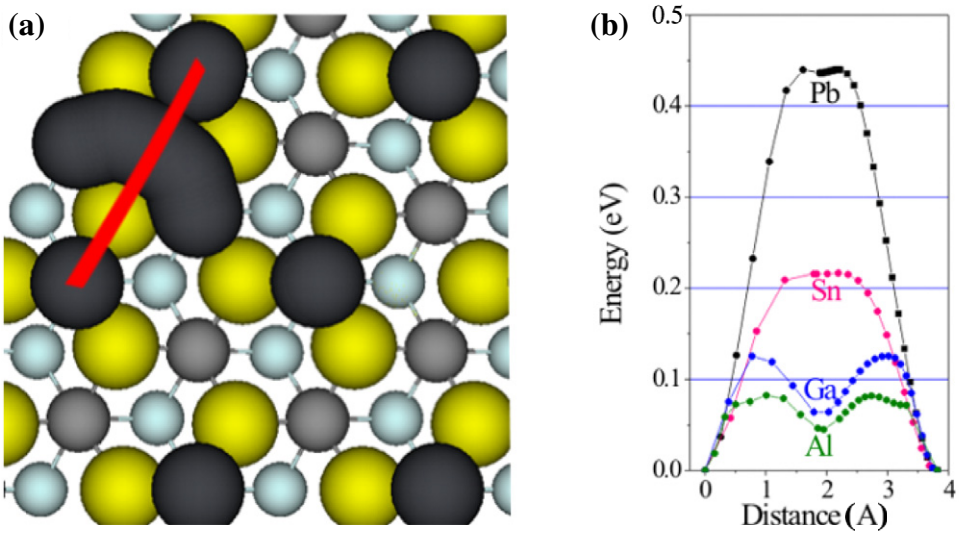

Figure 3. (a) The minimum energy path of the extra Me adatom diffusion on the corresponding Me-induced Si(111) $\sqrt{3} \times \sqrt{3}$ surface, which was obtained using NEB optimization, and (b) the corresponding energy profiles. The designations are identical to those in figure 1.

The diffusions of all extra Me adatoms under consideration have similar features, and using more images does not considerably affect the form of the diffusion path or the position of the saddle points, as observed in figure 3(b). In figure 3(b), the diffusion paths on the left of the symmetry plane were obtained using a sparse NEB grid, whereas the diffusion paths on the right of the symmetry plane were obtained using a fine NEB grid that contained 16–24 images. The resulting diffusion paths that were obtained for the maximum number of the NEB images almost coincide with the paths obtained using the grid with fewer images. The difference in the saddle point positions that were obtained using different NEB grids is less than 0.05 Å, and the difference between their energies is less than the error in the DFT calculations. The calculated activation energy barrier height for the extra Pb adatom is consistent with the experimental data obtained by Brihuega *et al* [2], which supports the single-adatom diffusion mechanism considered in this work. Similar calculations of the diffusion barriers of the other extra Me adatom diffusion give smaller activation energies for the smaller Me adatoms: Sn (0.36 eV), In (0.22 eV), Ga (0.13 eV) and Al (0.08 eV). Unfortunately, there are no experimental data for metals other than Pb with which to compare these values. However, the consistency between the calculated data and the experiment in the Pb case gives hope that the obtained results can predict the behaviour of the other extra Me adatoms on the similar surfaces.

Because the accuracy of the determination of the saddle point is important for FOTS calculations, the dimer method [39, 40] was used to search for the exact positions of the saddle points. This method gives an energy within ±0.5 meV of that obtained using the climbing NEB calculations, and the positions are within 0.05 Å for all investigated metals except Al. For the extra Al adatom diffusion, the uncertainty of the saddle point locations is higher (≈ 0.1 Å) because of the high mobility of the loosely bonded Al adatoms, but the uncertainty of their energies remains less than 0.5 meV. The diagonalized force constant matrix $\mathbf{D} = \| M_i^{-1/2} \Phi_{i,j} M_j^{-1/2} \|$ that was calculated at all of these saddle points has one negative value, which proves that these saddle points are true FOTSs.

Table 2. The dependence of the activation energy barrier height (eV) on the exchange-correlation potential that was used. In the last column, the minimal Me–Me dimer length (Å), which was attained at the middle of the diffusion path, is shown.

	Exchange-correlation potential				
Adatom	LDA	GGA PW91	GGA PBE	GGA PBEsol	Dimer length
Pb	0.44	0.42	0.42	0.42	3.05
Sn	0.36	0.34	0.35	0.33	2.95
In	0.23	0.21	0.21	0.22	3.0
Ga	0.13	0.11	0.12	0.13	2.6
Al	0.08	0.05	0.03	0.07	2.6
Bi	−1.55	–	–	–	2.95

As we can see in figure 3(b), two saddle points in the energy profile curves are separated from each other by a plateau, whose length is varied from ≈ 0.8 Å for the largest adatom Pb to ≈ 2.6 Å for the smallest adatom Al. The diffusion process is accompanied by the breaking of an Me–Si bond and an appreciable increase in the total energy from the minimal value to the maximal value when the extra Me adatom moves from the equilibrium T_4 position to the first saddle point. Subsequently, an Me–Me dimer is formed, whose bond length is determined by the Me atomic size and the energy that passes through the maximum value. For larger Me adatoms such as Pb, Sn and In, the Me–Me dimer length is ≈ 3.0 Å; for smaller Me adatoms such as Ga and Al, it is ≈ 2.6 Å, as shown in table 2. Thus, because the smaller Me atoms can come closer to each other without considerable repulsion, the corresponding energy barrier is smaller, and the distance between the saddle points is much larger. After the extra Me adatom passes the second saddle point, the reverse process takes place: the Me–Me dimer is broken, and a new Me–Si bond is formed with a consequent decrease in energy to the corresponding minimum value. Thus, the distance between the saddle points is determined by the minimum possible distance between two Me adatoms: the moving Me adatom and the closest Me adatom in the T_4 position.

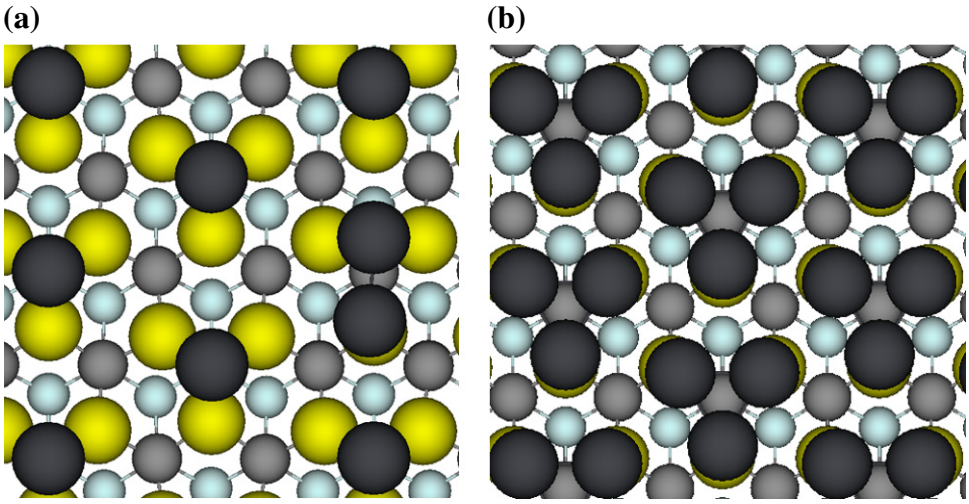

Figure 4. (a) The structure of the optimized Bi-induced Si(111) $\sqrt{3} \times \sqrt{3}$ 1/3 ML surface with one extra Bi adatom and (b) the structure of the optimal Bi-induced Si(111) $\sqrt{3} \times \sqrt{3}$ 1 ML surface.

The behaviour of the extra Bi adatom on an Si(111) $\sqrt{3} \times \sqrt{3}$–Bi surface is completely different and cannot be compared with the other extra Me adatom diffusion. The main reason is that a shift of the extra Bi adatom to the centre of the diffusion path, which is accompanied by a Bi–Bi dimer formation (see figure 4(a)), results in an appreciable dip in the energy. This energy is 1.55 eV lower than the energy of the state with the extra Bi adatom in the T_4 site, which implies that the T_4 site state is not a ground state for the Si(111) $\sqrt{3} \times \sqrt{3}$–Bi surface with an extra Bi adatom. This finding is supported by the calculations of the magic layer thickness in Bi ultrathin films on Si(111) surfaces by Saito *et al* [41]. They demonstrated that the most stable geometry of the β-phase of the Si(111) $\sqrt{3} \times \sqrt{3}$–Bi surface is the so-called milkstool structure, which consists of Bi trimers centred at the T_4 sites, as shown in figure 4(b). Because the milkstool structure has three Bi atoms per $\sqrt{3} \times \sqrt{3}$ cell, whereas the 1/3 ML structure that has been considered has one Me adatom, we can compare their formation energies using only the cohesive energy of bulk Bi μ_{Bi}:

$$\Delta E = E_{4\sqrt{3}\times 4\sqrt{3}-1/3\,\mathrm{ML+Bi\ adatom}} + \Delta n\,\mu_{\mathrm{Bi}} - E_{4\sqrt{3}\times 4\sqrt{3}-1\,\mathrm{ML}}, \quad (1)$$

where Δn is the difference between the number of Bi adatoms in the $\sqrt{3} \times \sqrt{3}$-1/3 ML and the $\sqrt{3} \times \sqrt{3}$-1 ML surface structures.

The calculation shows that the milkstool structure is more favourable by $\Delta E = 0.55$ eV per 1×1 cell than the $\sqrt{3} \times \sqrt{3}$ 1/3 ML structure with an extra Bi adatom. Thus, the Bi adatoms prefer to form dimers, as in our case of the extra Bi adatom on the 1/3 ML $\sqrt{3} \times \sqrt{3}$ surface. We can expect that this peculiarity is intrinsic to Bi. Indeed, the calculation of the milkstool structure for the other metals with one ML coverage on the Si(111) $\sqrt{3} \times \sqrt{3}$ surface shows that the trimmers break and the Me adatoms become chaotically disordered.

The dependence of the diffusion on the exchange-correlation potential was investigated by performing a series of GGA calculations for the PW91 [42], PBE [43] and PBEsol [44] exchange correlations. The form of the reaction path and the energy barrier profiles are almost identical to those obtained using the LDA functional, which are shown in figure 3. In table 2, the height of the activation barriers are compared based on the exchange-correlation types. We observe that the GGA functional gives a smaller value for the activation energy for all of the considered extra Me adatom diffusions. The overall difference in the activation barrier value given by the different exchange-correlation potentials is not more than 0.03 eV for all considered Me adatoms. Although this difference is quite large for the lighter Me adatom—it constitutes one-third of the activation barrier heights for the Al adatom diffusion. In the latter case, the GGA can be expected to give worse results than the LDA. Regarding the Sn adatom, Flores *et al* [45] and Ortega *et al* [46] showed the importance of many-body electron correlations in the Si(111) $\sqrt{3} \times \sqrt{3}$ Sn-induced surface. They demonstrated that the correlations leads to the formation of a stable narrow-gap Mott–Hubbard insulating state. The inclusion of the on-site Coulomb interaction L(S)DA+U with the parameters $U = 1.5$ eV and $J_{nn} = 0.35$ eV, which were reported by Ortega *et al* [46], slightly enlarges the activation barrier heights to 0.37 eV, which is not too different from the initial LDA results.

Table 3. The dependence of the prefactor logarithm on the atomic displacement Δu (Δx_i, Δy_i, Δz_i) and the kinetic energy cutoff E_{cut}.

Displacement (Å)	Prefactor logarithm		
$\Delta x_i = \Delta y_i = \Delta z_i$	$E_{\mathrm{cut}} = 300$ eV	$E_{\mathrm{cut}} = 350$ eV	$E_{\mathrm{cut}} = 400$ eV
0.005	28.9	27.3	28.7
0.01	28.5	28.8	28.4
0.02	27.8	27.7	27.7
0.03	27.6	27.5	27.6
0.04	27.4	27.7	–

3.3. Phonon calculations

The prefactor calculation is one of the most challenging tasks in surface dynamics. As seen from equation (A.2), the calculation requires very precise values of the phonon frequencies because they enter the prefactors factors exponentially. The calculation also requires a sufficiently

Table 4. The dependence of the prefactor logarithm that was obtained for the atomic displacement $\Delta x_i = \Delta y_i = \Delta z_i = 0.005$ Å and the kinetic energy cutoff $E_{cut} = 300$ eV on the number of moving atoms, which were taken for the phonon calculations.

Number of atoms	1	2	5	7	27	50	100	150	209
Prefactor logarithm	27.4	27.6	27.6	27.5	27.7	28.0	28.6	28.7	28.9

large number of degrees of freedom (the moving atoms) because the number of factors in the prefactor is equal to the number of degrees of freedom. A high precision of the calculated prefactor is often not necessary because its precise experimental measurements are difficult and generally performed in a narrow temperature range, where the error is deliberately larger than the calculated values. As shown in the appendix, the prefactor for a single-atomic diffusion is several orders of magnitude larger than the prefactor for a collective-atomic diffusion. Therefore, the precision of one–two orders of magnitude would be sufficient to clarify the diffusion mechanism.

The prefactor was calculated using equation (A.2), which contains the vibrational frequencies of all relaxing (not fixed) atoms in the ground equilibrium state and in the FOTS. The temperature in equation (A.2) was the average of the temperatures that were used by Brihuega *et al* [2] to experimentally determine the prefactor $T = \frac{165+145}{2}$ K for the extra Pb adatom diffusion on the corresponding Pb-induced Si(111) $\sqrt{3} \times \sqrt{3}$ surface. The dependence of the calculated prefactor logarithm on the kinetic energy cutoff and the value of the atomic displacements used for calculations are shown in table 3. The logarithm of the prefactor, which is given by the atomic displacements in the range 0.005–0.03 Å, is within 27.3–28.9. The corresponding prefactor value varies within $1–3 \times 10^{12}$ Hz, which is of the same order of magnitude as the experimental value $10^{13.0 \pm 0.4}$ Hz. Similar to its dependency on the atomic displacements value, the prefactor logarithm depends on the number of the moving atoms that were taken for the phonon frequency calculation, as shown in table 4, which introduces an error of the same order of magnitude. In table 5, to eliminate the additional error introduced by the small number of considered phonon frequencies, the prefactors were obtained for all relaxing (not fixed) atoms that were taken for the phonon calculations.

Thus, by considering the contributions of all moving atoms, we obtained the correct order of magnitude of the Arrhenius prefactor for the extra Pb adatom diffusion on the corresponding Si(111) $\sqrt{3} \times \sqrt{3}$–Pb surface. Because of the precision of these calculations, the prefactor values cannot be compared quantitatively, but such precision supports the assumed mechanism of the single-atomic diffusion for the experimentally observed extra Pb adatom movement. Otherwise, the prefactor value would be different from the experimental value by several orders of magnitude. The prefactor that was calculated for the other Me adatoms using the same technique is also in the same order of magnitude of $\sim 10^{11-13}$ Hz, as shown in table 5. It appears that the exchange correlation potential appears does not considerably affect the prefactor values.

From the calculated vibration frequencies, we can estimate the contribution of the zero-point phonon effect to the activation energy using the following approximations for the zero-point energies of the equilibrium state and the transition states: $E_0 = \sum_{i=1}^{3N} \frac{\hbar\omega_i}{2}$ and $E_T = \sum_{i=1}^{3N-1} \frac{\hbar\omega_i^*}{2}$, respectively. The zero-point phonon effect contribution $|E_0 - E_T|$ varies from 2 meV for the Al adatom to l4 meV for the Sn adatom for $E_{cut} = 300$ eV and atomic displacement $\Delta x_i = \Delta y_i = \Delta z_i = 0.01$ Å. This low contribution of the phonon energy to the total energy difference indicates that the NEB optimized transition states are near the true saddle point with the minimal energy.

Table 5. The dependence of the prefactor on the exchange-correlation potential. The prefactor was obtained for the atomic displacement $\Delta x_i = \Delta y_i = \Delta z_i = 0.01$ Å and the kinetic energy cutoff $E_{cut} = 300$ eV.

	Exchange-correlation potential			
Adatom	LDA	GGA PW91	GGA PBE	GGA PBEsol
Pb	2.4×10^{12}	6.2×10^{11}	1.3×10^{12}	1.7×10^{12}
Sn	2.8×10^{12}	1.1×10^{12}	1.3×10^{12}	1.2×10^{12}
In	7.1×10^{11}	4.2×10^{12}	5.9×10^{12}	3.4×10^{11}
Ga	7.9×10^{11}	8.1×10^{11}	7.9×10^{11}	7.7×10^{11}
Al	9.9×10^{11}	1.0×10^{12}	9.8×10^{11}	–

4. Conclusion

The DFT calculations of the extra Me adatom diffusion on the corresponding Me-induced Si(111) $\sqrt{3} \times \sqrt{3}$ surface demonstrate that the height of the activation energy barrier strongly depends on the Me atomic radius. The larger Me adatoms cannot approach one another without considerable repulsion, which is followed by an increase in the total energy. The minimum Me–Me distance is as much as about 3.1 Å for the largest (Pb) Me adatoms and as little as about 2.6 Å for the smallest (Al) Me adatoms. The smaller adatoms are more mobile, and the corresponding activation energy barriers are appreciably smaller and wider. The barrier consists of two saddle points that are separated by approximately 2.5 Å for the smaller Me adatoms such as Al and Ga and 0.6–0.8 Å, for the large Me adatoms such as Pb. The Arrhenius prefactors, which were obtained with different precisions and atomic displacements in different exchange-correlation approximations, are $\sim 10^{11-13}$ Hz for all investigated surfaces. This result supports the considered single-adatom diffusion model.

Acknowledgments

This work was supported by the Russian Foundation for Basic Research (grants nos. 11-02-98516 and 12-02-00416) and the Ministry of Education and Science of the Russian Federation (grants nos. 8022, 8581, 2.1004.2011 and Nsh-774.2012.2). All calculations were performed using the facilities of the collective computing centre of the Far Eastern Computational Resource[1].

[1] Far-eastern computational resources for collective use: www.cc.dvo.ru.

Appendix. Diffusion parameters calculation

Diffusion can be simply classified as either interstitial or substitutional based on the location of the impurity atom. Interstitial diffusion is usually representative for the bulk solid, whereas substitutional diffusion more often occurs at the surface because the atoms move from one atomic site to another. In a perfect lattice, this diffusion would require the atoms to swap places within the lattice. A straight-forward swapping of atoms would require a lot of energy because the swapping atoms would need to physically push other atoms out of the way to swap places. In practice, a substitutional diffusion occurs only if there are vacancies at the surface. If a vacancy is present, one of the adjacent atoms can move into the vacancy and creates a vacancy in its original site. Diffusion through one vacancy is said to be vacancy mediated. Such diffusion is responsible for the mobility of In adatoms on a Cu(100) surface [47], the mass transport between adatom islands on Cu(001) [48] and the Me–Si adatom exchange on Me-induced Si(111) $\sqrt{3}\times\sqrt{3}$ surfaces [49].

One key characteristic of diffusion is the number of participating atoms, which is difficult to detect using modern experimental techniques such as STM. For example, in the orchestrated exchange discovered by Kaxiras and Erlebacher [50], the number of atoms participating in the diffusion is much larger than the number of atoms that are seen moving in the STM. The orchestrated exchange mechanism implies a division of adatoms into three types: 'spectators', 'enablers' and 'movers'. The 'spectators' do not participate in the exchange but they are necessary for the diffusion to occur. The 'enablers' must move for the exchange to occur, but they end up in the same position after the exchange, being indistinguishable experimentally. Hence, the only visible moving adatoms are the 'movers', which end up in different positions after the exchange. If the energy dissipation rate is nearly constant, and the dissipation of the extra thermal energy is sufficiently fast, then the adsorbate particle will vibrate near a nearest-neighbour site and the jump length distribution should be an exponentially decaying Arrhenius function of the distance:

$$\nu = \nu_0 \mathrm{e}^{-E_\mathrm{d}/kT}, \tag{A.1}$$

where ν is the adatom hopping rate, E_d is the diffusion activation energy, k is the Boltzmann's constant, T is the temperature and ν_0 is the pre-exponential factor or the prefactor.

The Arrenius prefactor ν_0 can be regarded as a simple indicator of the diffusion mechanism because it is proportional to the diffusion probability. The probability of the collective-atomic diffusion $P_\mathrm{collective}$ is clearly defined by the product of the diffusion probabilities P_adatom of every adatom movement that participates in the diffusion:

$$P_\mathrm{collective} \sim P_{\mathrm{adatom}_1} \cdot P_{\mathrm{adatom}_2} \cdot P_{\mathrm{adatom}_3} \cdots .$$

Hence, the probability of the collective diffusion must be several orders of magnitude smaller than the probability of a single-atomic diffusion. In practice, only accurate, time-consuming calculations can give reliable values of the prefactor that is directly comparable with the experimental values, and only the present state of development of supercomputing facilities allows us to perform such calculations.

The quantum mechanical solution of the harmonic oscillator yields the harmonic transition state theory (hTST) jump rate:

$$\nu_0 = \frac{kT}{h}\frac{\prod_{i=1}^{3N}\left(1-\mathrm{e}^{\frac{-\hbar\omega_i}{kT}}\right)}{\prod_{i=1}^{3N-1}\left(1-\mathrm{e}^{\frac{-\hbar\omega_i^*}{kT}}\right)}, \tag{A.2}$$

where N is the number of atoms, $h(\hbar)$ is Planck's constant, and ω_i and ω_i^* are the real normal modes of vibration on the ground state and the activation state, respectively. On a saddle point, there is one fewer real normal mode than in the ground state because the negative curvature yields an imaginary frequency ω_i^* in the direction of the reaction coordinate.

In the high-temperature region, i.e. $kT \gg \hbar\omega$, equation (A.2) becomes the result of Vineyard [51] for the classical harmonic oscillator:

$$\nu_0 = \frac{kT}{h}\frac{\prod_{i=1}^{3N}\omega_i}{\prod_{i=1}^{3N-1}\omega_i^*}. \tag{A.3}$$

Considering the large error of the experimentally determined prefactor, this result appears notably acceptable. In this paper, the unsimplified form of equation (A.2) is used to avoid any error that is introduced by neglecting quantum effects.

Consequently, the consistency between the experimental prefactor and the calculated prefactor for the chosen diffusion mechanism would indicate that the chosen mechanism is correct. However, the prefactor calculation is notably time-consuming because the number of factors in equations (A.2)–(A.3) is equal to the number of degrees of freedom, which is three times greater than the number of relaxing atoms, and each of these factors needs a separate self-consistent calculation at a fixed geometry. Sometimes, one confines oneself to several terms of this product [52], which can be justified by the low precision of the experimentally determined prefactor with which the calculated value is compared.

All phonon frequencies in equation (A.2) were calculated using the harmonic approximation in the Born–von Karman theory, where the total energy of a system is expanded in the atomic displacement, and only the linear terms are preserved:

$$E = E_0 + \sum_i f_i u_i + \frac{1}{2}\sum_{i,j}\Phi_{i,j}u_i u_j, \tag{A.4}$$

where u_i is the atomic displacement, E_0 is the total energy at zero atomic displacement and f_i is the Cartesian component of the force that acts on the ith atom, which is equal to zero in mechanical equilibrium. The index i in equations (A.2) and (A.4) refers to all degrees of freedom of all non-fixed atoms in the cell. The matrix $\Phi = \|\Phi_{i,j}\|$ is the force constant matrix that defines the dynamical matrix $\mathbf{D} = \| M_i^{-1/2}\Phi_{i,j}M_j^{-1/2} \|$, where M_i is the mass associated with the ith atom. Diagonalizing matrix D, we obtained the squares of all phonon frequencies that enter into equation (A.2) using VASP transition state theory tools[2]. The

[2] Vasp TST tools: http://theory.cm.utexas.edu/vtsttools.

number of real and imaginary frequencies can be used as a direct criterion of the accuracy of the ground state and the FOTS calculations.

References

[1] Brihuega I, Custance O, Ugeda M M and Gómez-Rodríguez J M 2007 *Phys. Rev.* B **75** 155411
[2] Brihuega I, Ugeda M M and Gómez-Rodríguez J M 2007 *Phys. Rev.* B **76** 035422
[3] Lifshits V G, Oura K, Saranin A A and Zotov A V 2001 *Metals on Semiconductors in Physics of Covered Solid Surfaces (New Series)* (*Group III: Condensed Matter* vol 42) ed H Landolt and R Börnstein (Berlin: Springer) pp 259–419
[4] Chelikowsky J R 1977 *Phys. Rev.* B **16** 3618
[5] Northrup J E 1984 *Phys. Rev. Lett.* **53** 683
[6] Meade R D and Vanderbilt D 1989 *Phys. Rev. Lett.* **63** 1404
[7] Zegenhagen J, Patel J R, Freeland P, Chen D M, Golovchenko J A, Bedrossian P and Northrup J E 1989 *Phys. Rev.* B **39** 1298
[8] Nicholls J M, Mårtensson P, Hansson G V and Northrup J E 1985 *Phys. Rev.* B **32** 1333
[9] Chan T-L, Wang C Z, Hupalo M, Tringides M C, Lu Z-Y and Ho K M 2003 *Phys. Rev.* B **68** 045410
[10] Ramchurn S K, Bird D M and Bullett D W 1990 *J. Phys.: Condens. Matter* **2** 7435
[11] Cheng C and Kunc K 1997 *Phys. Rev.* B **56** 10283
[12] Hammer B, Scheffler M, Jacobsen K W and Nørskov J K 1994 *Phys. Rev. Lett.* **73** 1400
[13] Penev E, Kratzer P and Scheffler M 1999 *J. Chem. Phys.* **110** 3986
[14] Tran F, Laskowski R, Blaha P and Schwarz K 2007 *Phys. Rev.* B **75** 115131
[15] Furthmüller J, Hafner J and Kresse G 1994 *Phys. Rev.* B **50** 15606
[16] Jia Y, Wu B, Li C, Einstein T L, Weitering H H and Zhang Z 2010 *Phys. Rev. Lett.* **105** 066101
[17] Northrup J E 1989 *Phys. Rev.* B **39** 1434
[18] Teng J, Zhang L, Jiang Y, Guo J, Wang E, Ebert P, Sakurai T and Wu K 2010 *J. Chem. Phys.* **133** 014704
[19] Dai X-Q, Ju W-W, Wang G T and Xie M N 2004 *Surf. Sci.* **572** 77
[20] Erwin S C, Baski A A, Whitman L J and Rudd R E 1999 *Phys. Rev. Lett.* **83** 1818
[21] Yeom H W, Yoo K and Oh D-H 2011 *Surf. Sci.* **605** 146
[22] Profeta G, Ottaviano L, Santucci S and Continenza A 2002 *Phys. Rev.* B **66** 081303
[23] Koroteev Y M, Bihlmaver G, Chulkov E V and Blügel S 2008 *Phys. Rev.* B **77** 045428
[24] Owen J H G, Miki K and Bowler D R 2003 *Surf. Sci.* **527** L177
[25] Goedecker S and Maschke K 1992 *Phys. Rev.* A **45** 88
[26] Kresse G and Hafner J 1993 *Phys. Rev.* B **47** 558
[27] Kresse G and Hafner J 1994 *Phys. Rev.* B **49** 14251
[28] Kresse G and Furthmüller J 1996 *Phys. Rev.* B **54** 11169
[29] Kresse G and Furthmüller J 1996 *Comput. Mater. Sci.* **6** 15
[30] Hohenberg P and Kohn W 1964 *Phys. Rev.* **136** B864
[31] Kohn W and Sham L J 1965 *Phys. Rev.* **140** A1133
[32] Blöchl P E 1994 *Phys. Rev.* B **50** 17953
[33] Kresse G and Joubert D 1999 *Phys. Rev.* B **59** 1758
[34] Ceperley D M and Alder B J 1980 *Phys. Rev. Lett.* **45** 566
[35] Perdew J P and Zunger A 1981 *Phys. Rev.* B **23** 5048
[36] Henkelman G, Uberuaga B P and Jonsson H 2000 *J. Chem. Phys.* **113** 9901
[37] Henkelman G and Jonsson H 2000 *J. Chem. Phys.* **113** 9978
[38] Sheppard D, Terrell R and Jónsson H 2008 *J. Chem. Phys.* **128** 134106
[39] Kästner J and Sherwood P 2008 *J. Chem. Phys.* **128** 014106
[40] Heyden A, Bell A T and Keil F J 2005 *J. Chem. Phys.* **123** 224101
[41] Saito M, Ohno T and Miyazakia T 2004 *Appl. Surf. Sci.* **237** 80
[42] Wang Y and Perdew J P 1991 *Phys. Rev.* B **44** 13298
[43] Perdew J P, Burke K and Ernzerhof M 1996 *Phys. Rev. Lett.* **77** 3865
[44] Perdew J P, Ruzsinszky A, Csonka G I, Vydrov O A, Scuseria G E, Constantin L A, Zhou X and Burke K 2008 *Phys. Rev. Lett.* **100** 136406
[45] Flores F, Ortega J, Pérez R, Charrier A, Thibaudau F, Debever J M and Themlin J M 2001 *Prog. Surf. Sci.* **67** 299
[46] Ortega J, Pérez R and Flores F 2002 *J. Phys.: Condens. Matter* **14** 5979
[47] van Gastel R, Somfai E, van Albada S B, van Saarloos W and Frenken J W M 2001 *Phys. Rev. Lett.* **86** 1562
[48] Hannon J B, Klünker C, Giesen M, Ibach H, Bartelt N C and Hamilton J C 1997 *Phys. Rev. Lett.* **79** 2506
[49] Luniakov Yu V 2011 *Surf. Sci.* **605** 1866
[50] Kaxiras E and Erlebacher J 1994 *Phys. Rev. Lett.* **72** 1714
[51] Vineyard G H 1957 *J. Phys. Chem. Solids* **3** 121
[52] Fedorov A S, Popov Z I, Kuzubov A A and Ovchinnikov S G 2012 *JETP Lett.* **95** 143